HERBERT WALTHER
Max-Planck-Institut für Quantenoptik

QUANTUM PHENOMENA OF SINGLE ATOMS

Conferenza tenuta il 14 ottobre 1997

ABSTRACT. In this paper recent experiments performed in our laboratory are reviewed dealing with the investigation of quantum phenomena in the radiation interaction of single atoms. The first part describes experiments in single mode cavities using the one-atom maser or micromaser and in the second part experiments with ion traps are summarized. The latter experiments concentrate on the investigation of resonance fluorescence. In addition new experimental proposals using ultracold atoms in cavities and traps are discussed. In those future experiments the interplay between atomic waves and light waves is important and leads to new phenomena in radiation-atom interaction.

1 Introduction

Laser spectroscopy techniques allow today to observe quantum phenomena in radiation-atom interaction on the basis of single atoms. The most suitable systems in this connection seem to be single atoms in cavities and also single atoms in traps. The studies in cavities allow to select one interacting mode and thus represent the ideal system with respect to a quantum treatment. In high Q cavities a steady state field of photons can be generated displaying non-classical photon statistics. It thus gets possible to study the interaction also in the limit of non-classical or sub-Poissonian fields. Single trapped ions allow to observe among other phenomena quantum jumps and antibunching in fluorescence radiation. In general the fluorescent channel represents an interaction with many modes, however, it is also possible to combine single mode cavities with trapped atoms as it is e.g. the case in the proposed ion-trap laser.

In such a setup many new phenomena not observable in the one-atom maser get accessible.

A new and interesting twist in radiation-atom interaction can be added when ultracold atoms are used in both cavities and traps. In this case the distribution of the matter wave plays an important role besides the standing electromagnetic wave in the cavity and their interaction is determined by their respective overlap leading to new effects.

In the following we will review experiments of single atoms in cavities and traps performed in our laboratory. Furthermore new proposals for experiments with ultracold atoms will be discussed. We start with the discussion of the one-atom maser.

2 Experiments with the One Atom Maser

The one-atom maser or micromaser uses a single mode of a superconducting niobium cavity [1-4]. In the experiments values of the quality factor as high as 3×10^{10} have been achieved for the resonant mode, corresponding to an average lifetime of a photon in the cavity of 0.2 s. The photon lifetime is thus much longer than the interaction time of an atom with the maser field; during the atom passes through the cavity the only change of the cavity field that occurs is due to the atom-field interaction. Contrary to other strong coupling experiments in cavities (optical or microwave), see e.g. H. J. Kimble et al. [5] for a comparison between the different setups, it is possible with our micromaser to generate a steady state field in the cavity which has nonclassical properties so that the interaction of single atoms in those fields can be investigated. Furthermore the generation process of those fields has been studied and is well understood. The experiments is quite unique in this respect; this also holds in comparison with the one-atom laser [6] which has been omitted in the survey given in Table 1 of Ref. [5].

The atoms used in our micromaser experiments are rubidium Rydberg atoms pumped by laser excitation into the upper level of the maser transition, which is usually induced between neighboring Rydberg states. In the experiments the atom-field interaction is probed by observing the population in the upper and lower maser levels after the atoms have left the cavity. The field in the cavity consists only of single or a few photons depending on the atomic flux. Nevertheless, it is possible to study the interaction in considerable detail. The dynamics of the atom-field interaction treated with the Jaynes-Cummings model was investigated by selecting and varying the velocity of the pump atoms [2]. The counting statistics of the pump atoms emerging from the cavity allowed us to measure the non-classical character of the cavity field [3, 4] predicted by the micromaser theory. The maser field can be investigated in this way since there is entanglement between the maser field and the state in which the atom leaves the cavity [7, 8]. It also has been observed that under suitable experimental conditions the maser field exhibits metastability hysteresis [9]. The first of the maser

experiments have been performed at cavity temperatures of 2 or 0.5 K. In the more recent experiments the temperature was reduced to roughly 0.1 K by using an improved setup in a dilution refrigerator [9]. For a review of the previous work see Raithel et. al. [11].

In the following we give a brief review of recent experiments which deal with the observation of quantum jumps of the micromaser field [9] and with the observation of atomic interferences in the cavity [10]. New experiments on the correlation of atoms after the interaction with the cavity field will be briefly mentioned. We will also discuss new possibilities opened up when ultracold atoms are used for the experiments.

2.1 Quantum Jumps and Atomic Interferences in the Micromaser

Under steady-state conditions, the photon statistics P(n) of the field of the micromaser is essentially determined by the pump parameter, $\Theta = \mathrm{N}_{ex}^{1/2}\Omega \cdot \mathrm{t}_{int}/2$ [11, 13]. Here, N_{ex} is the average number of atoms that enter the cavity during $\tau_{cav}\Omega$, the vacuum Rabi floppy frequency, and t_{int} is the atom-cavity interaction time. The quantity $\langle \nu \rangle = \langle n \rangle / N_{ex}$ shows the following generic behavior (see Fig. 1): It suddenly increases at the maser threshold value $\Theta = 1$, and reaches a maximum for $\Theta \approx 2$ (denoted by A in Fig. 1). At threshold the characteristics of a continuous phase transition [12,13] are displayed. As Θ further increases, $\langle \nu \rangle$ decreases and reaches a minimum at $\Theta \approx 2\pi$, and then abruptly increases to a second maximum (B in Fig. 1). This general type of behavior recurs roughly at integer multiples of 2π, but becomes less pronounced with increasing Θ. The reason for the periodic maxima of $\langle \nu \rangle$ is that for integer multiples of $\Theta = 2\pi$ the pump atoms perform an almost integer number of full Rabi flopping cycles, and start to flip over at a slightly larger value of Θ, thus leading to enhanced photon emission. The periodic maxima in $\langle \nu \rangle$ for $\Theta = 2\pi, 4\pi$, and so on can be interpreted as first-order phase transitions [12,13]. The field strongly fluctuates for all phase transitions being caused by the presence of two maxima in the photon number distribution P(n) at photon numbers n_l and $n_h (n_l < n_h)$.

The phenomenon of the two coexisting maxima in P(n) was also studied in semiheuristic Fokker-Planck (FP) approach [12]. There, photon number distribution P(n) is replaced by a probability function $P(\nu, \tau)$ with continuous variables $\tau = t/\tau_{cav}$ and $\nu(n) = n/N_{ex}$, the latter replacing the photon number n. The steady-state solution obtained for $P(\nu, \tau), \tau \gg 1$, can be constructed by means of an effective potential $V(\nu)$, showing minima at positions where maxima of $P(\nu, \tau), \tau \gg 1$, are found. Close to $\Theta = 2\pi$ and multiples thereof, the effective potential $V(\nu)$ exhibits two equally attractive minima located at stable gain-loss equilibrium points of maser operation [14] (see Fig. 1). The mechanism at the phase transition mentioned is always the same: A minimum of $V(\nu)$ loses its global character when Θ

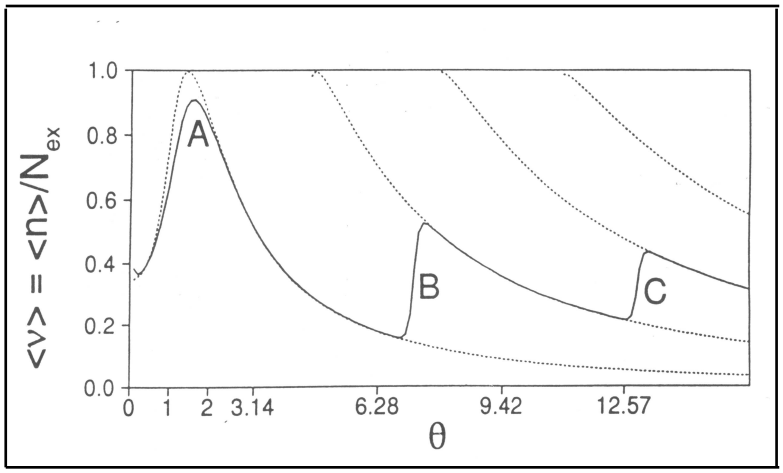

Figure 1: *Mean value of $\nu = n/N_{ex}$ versus the pump parameter $\Theta = \Omega t_{int}\sqrt{N_{ex}}/2$, where the value of Θ is changed via N_{ex}. The solid line represents the micromaser solution for Ω = 36 kHz, t_{int}= 35μs, and temperature T=0.15 K. The dotted lines are semiclassical steady-state solutions corresponding to fixed stabel gain=loss equilibrium photon numbers [14]. The crossing points between a line Θ =const and the dotted lines correspond to the values where minima in the Fokker-Planck potential $V(\nu)$ occur.*

is increased, and is replaced in this role by the next one. This reasoning is a variation of the Landau theory of first-order phase transitions, with $\sqrt{\nu}$ being the order parameter. This analogy actually leads to the notion that in the limit $N_{ex} \to \infty$ the change of micromaser field around integer multiples $\Theta = 2\pi$ can be interpreted as first-order phase transitions.

Close to first-order phase transitions long field evolution time constants are expected [12, 13]. This phenomenon was experimentally demonstrated in Ref. [9], as well as related phenomena, such as spontaneous quantum jumps between equally attractive minima of $V(\nu)$, bistability, and hysteresis. Some of those phenomena are also predicted in the two-photon micromaser [15], for which qualitative evidence of first-order phase transitions and hysteresis is reported.

The experimental setup used is shown in Fig. 2. It is similar to that described by Rempe and Walther [4] and Benson, Raithel and Walther [9]. As before ^{85}Rb atoms were used to pump the maser. They are excited from the $5S_{1/2}$, F= 3 ground state to $63P_{3/2}$, $m_J = \pm 1/2$ states by linearly polarized light of a frequency-doubled c.w. ring dye laser. The polarization of the laser light is linear and parallel to the likewise linearly polarized maser field, and therefore only $\Delta m_J = 0$ transitions are excited. Superconducing niobium cavities resonant with the transition to the $61D_{3/2}$,$m_J = \pm 1/2$

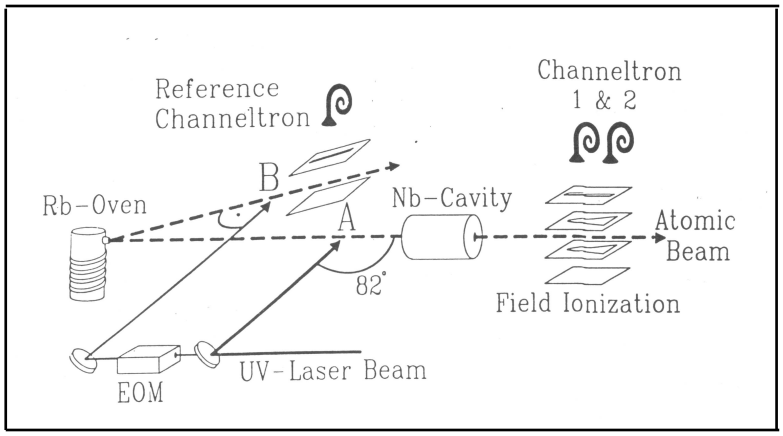

Figure 2: *Sketch of the experimental setup. The rubidium atoms emerge from an atomic beam oven and are excited at an angle of 82° at location A. After interaction with the cavity field, they enter a state-selective field ionization region, where channeltrons 1 and 2 detect atoms in the upper and lower maser levels, respectively. A small fraction of the UV radiation passes through an electro-optic modulator (EOM), which generates sidebands of the UV radiation. The blueshifted sideband is used to stabilize the frequency of the laser onto the Doppler-free resonance monitored with a secondary atomic beam produced by the same oven (location B).*

states were used; the corresponding resonance frequency is 21.506 GHz. The experiments were performed in a ^{3}He/^{4}He dilution refrigerator with cavity temperatures $T \approx 0.15$K. The cavity Q values ranged from 4×10^9 to 8×10^9. The velocity of the Rydberg atoms and thus their interaction time t_{int} with the cavity field were preselected by exciting a particular velocity subgroup with the laser. For this purpose, the laser beam irradiated the atomic beam at an angle of approximately 82°. As a consequence, the UV laser light (linewidth $\approx$ 2MHz) is blueshifted by 50-200 MHz by the Doppler effect, depending on the velocity of the atoms.

Information on the maser field and interaction of the atoms in the cavity can be obtained solely by state-selective field ionization of the atoms in the upper or lower maser level after they have passed through the cavity. For different t_{int} the atomic inversion has been measured as a function of the pump rate by comparing the results with micromaser theory [12, 13], the coupling constant Ω is found to be $\Omega = (40 \pm 10)$ krad/s.

Depending on the parameter range, essentially three regimes of the field evolution time constant τ_{field} can be distinguished. Here we only discuss the results for intermediate time constants. The maser was operated under steady-state conditions close to the second first-order phase transition (C in Fig. 1). The interaction time was $t_{int} = 47\mu s$ and the cavity decay time

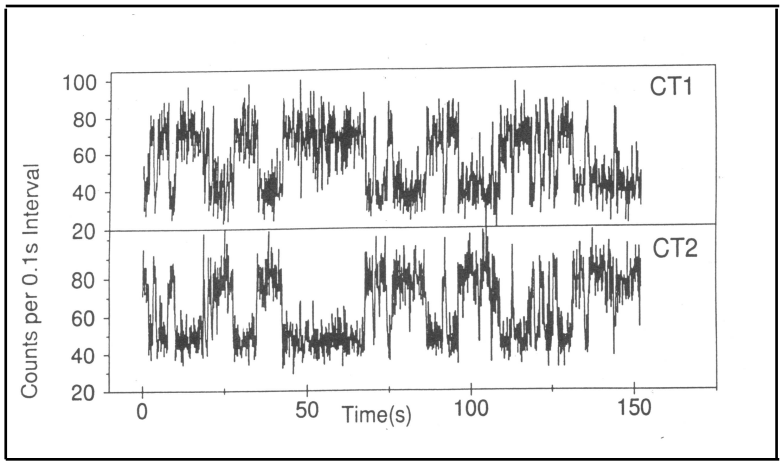

Figure 3: *Quantum jumps between two equally stable operation points of the maser field. The channeltron counts are plotted versus time (CT1= upper state and CT2= lower state signals). The signals of the two different detectors show a counterphase behavior; this makes it easy to discriminate between signal and noise.*

τ_{cav} = 60ms. The value of N_{ex} necessary to reach the second first-order phase transition was $N_{ex} \approx 200$. For these parameters, the two maxima in P(n) are manifested in spontaneous jumps of the maser field between the two maxima with a time constant of ≈ 5 s. This fact and the relatively large pump rate led to the clearly observable field jumps shown in Fig. 3. Because of the large cavity field decay time, the average number of atoms in the cavity was still as low as 0.17. The two discrete values for the counting rates correspond to the metastable operating points of the maser, which correspond to ≈ 70 and ≈ 140 photons. In the FP description, the two values correspond to two equally attractive minima in the FP potential $V(v)$. If one considers, for instance, the counting rate of lower-state atoms (CT2 in Fig. 3), the lower (higher) plateaus correspond to time intervals in the low (high) field metastable operating point. If the actual photon number distribution is averaged over a time interval containing many spontaneous field jumps, the steady-state result P(n) of the micromaser theory is recovered.

In the parameter ranges where switching occurs much faster than in the case shown in Fig. 3 the individual jumps cannot be resolved, therefore different methods have to be used for the measurement. Furthermore hysteresis is observed at the maser parameters for which the field jumps occur. Owing to lack of space these results cannot be discussed here. For a complete survey on the performed experiments it is referred to Ref. [9].

As next topic we would like to discuss the observation of atomic interferences in the micromaser [10]. Since a non-classical field is generated in

the maser cavity, we were able for the first time to investigate atomic interference phenomena under the influence of non-classical radiation; owing to the bistable behavior of the maser field the interferences display quantum jumps, thus the quantum nature of the field gets directly visible in the interference fringes. Interferences occur since a coherent superposition of dressed states is produced by mixing the states at the entrance and exit holes of the cavity. Inside the cavity the dressed states develop differently in time, giving rise to Ramsey-type interferences [16] when the maser cavity is tuned through resonance.

The setup used in the experiment is identical to the one described before [9]. However, the flux of atoms through the cavity is by a factor of 5-10 higher than in the previous experiments, where the 63 $P_{3/2}$ - $61D_{5/2}$ transition was used. For the experiments the Q-value of the cavity was 6×10^9 corresponding to a photon decay time of 42 ms.

Figure 4 shows the standard maser resonance in the uppermost plot which is obtained when the resonator frequency is tuned. At large values of N_{ex} ($N_{ex} > 89$) sharp, periodic structures appear. These typically consist of a smooth wing on the low-frequency side, and a vertical step on the high-frequency side. The clarity of the pattern rapidly decreases when N_{ex} increases to 190 or beyond. We will see later that these structures have to be interpreted as interferences. It can be seen that the atom-field resonance frequency is red-shifted with increasing N_{ex}, the shift reaching 200 kHz for $N_{ex} = 190$. Under these conditions there are roughly 100 photons on the average in the cavity. The large red-shift cannot be explained by AC Stark effect, which for 100 photons would amount to about one kHz for the transition used. Therefore it is obvious that other reasons must be responsible for the observed shift.

It is known from previous maser experiments that there are small static electric fields in the entrance and exit holes of the cavity. It is supposed that this field is generated by patch effects at the surface of the niobium metal caused by rubidium deposits caused by the atomic beam or by microcrystallites formed when the cavities are tempered after machining. The tempering process is necessary to achieve high quality factors. The influence of those stray fields is only observable in the cavity holes; in the center of the cavity they are negligible owing it the large atom-wall distances.

When the interaction time t_{int} between the atoms and the cavity field is increased the interference structure disappears for $t_{int} > 47\ \mu$s [10]. This is due to the fact that there is no non-adiabatic mixing any more between the substates when the atoms get too slow.

In order to understand the observed structures, the Jaynes-Cummings dynamics of the atoms in the cavity has to be analyzed. This treatment is more involved than that in connection with previous experiments, since the higher maser field requires detailed consideration of the field in the periphery of the cavity, where the additional influence of stray electric fields

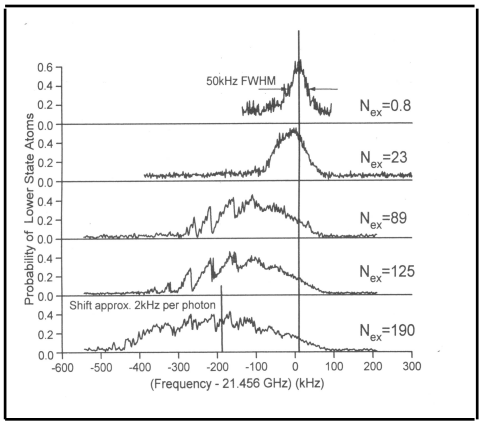

Figure 4: *Shift of the maser resonance 63 $P_{3/2}$ - 61 $D_{5/2}$ for fast atoms (t_{int} = 35μs). The upper plot shows the maser line for low pump rate ($N_{ex} < 1$). The FWHM linewidth (50kHz) sets an upper limit of ≈ 5 mV/cm for the residual electric stray fields in the center of the cavity. The lower resonance lines are taken for the indicated large values of N_{ex}. The plots show that the center of the maser line shifts by about 2 kHz per photon. In addition, there is considerable field-induced line broadening which is approximately proportional to $\sqrt{N_{ex}}$.For $N_{ex} \geq 89$ the lines display periodic structures, which are discussed in the text.*

is more important.

The usual formalism for the description of the coupling of an atom to the radiation field is the dressed atom approach [17], leading to splitting of the coupled atom-field states, depending on the vacuum Rabi-flopping frequency Ω, the photon number n, and the atom-field detuning δ. We face a special situation at the entrance and exit holes of the cavity. There we have a position-dependent variation of the cavity field, as a consequence of which Ω is position-dependent. An additional variation results from the stray electric fields in the entrance and exit holes. Owing to the Stark-effect these field lead to a position-dependent atom-field detuning δ.

The Jaynes-Cummings-Hamiltonian only couples pairs of dressed states. Therefore, it is sufficient to consider the dynamics within such a pair. In our case, prior to the atom-field interaction the system is in one of the two dressed states. For parameters corresponding to the periodic substructures in Fig. 4 the dressed states are mixed only at the beginning of the atom-field interaction and at the end. The mixing at the beginning creates a coherent superposition of the dressed states. Afterwards the system develops adiabatically, whereby the two dressed states accumulate a differential dynamic phase Φ which strongly depends on the cavity frequency. The mixing of the dressed states at the entrance and exit holes of the cavity, in combination with the intermediate adiabatic evolution, generates a

situation similar to a Ramsey two-field interaction.

The maximum differential dynamic phase Φ solely resulting from dressed state coupling by the maser field is roughly 4π under the experimental conditions used here. This is not sufficient to explain the interference pattern of Fig. 4, where we have at least six maxima corresponding to a differential phase of 12π. This means that an additional energy shift differently affecting upper and lower maser states is present. Such a phenomenon can be caused by the above mentioned small static electric fields present in the holes of the cavity. The static field causes a position-dependent detuning δ of the atomic transition from the cavity resonance; as a consequence we get an additional differential dynamic phase Φ. In order to interpret the periodic substructures as a result of the variation of Φ with the cavity frequency, the phase Φ has to be calculated from the atomic dynamics in the maser field.

The quantitative calculation can be performed on the basis of the micromaser theory. The calculations reproduce the experimental finding that the maser line shifts to lower frequencies when N_{ex} is increased [10]. The mechanism for that can be explained as follows: the high-frequency edge of the maser line does not shift with N_{ex} et all, since this part of the resonance is produced in the central region of the cavity, where practically non static electric fields are present. The low-frequency cutoff of the structure is determined by the location where the mixing of dressed states occurs. With decreasing cavity frequency those points shift closer to the entrance and exit holes, with the difference between the particular cavity frequency and unperturbed atomic resonance frequency giving a measure of the static electric field at the mixing locations. Closer to the holes the passage behaviour of the atoms through the mixing locations gets non-adiabatic for the following reasons: firstly, the maser field strength reduces towards the holes. This leads to reduced repulsion of the dressed states. Secondly, the stray electric field strongly increases towards the holes. This implies a larger differential slope of the dressed state energies at the mixing locations, and therefore leads to a stronger non-adiabatic passage. At the same time the observed signal extends further to the low frequency spectral region. Since the photon emission probabilities are decreasing towards lower frequencies their behaviour finally defines the low-frequency boundary of the maser resonance line. With increasing N_{ex} the photon number n increases. As for larger values of n the photon emission probabilities get larger, also increasing N_{ex} leads to an extension of the range of the signal to lower frequencies. This theoretical expectation is in agreement with the experimental observation.

In the experiment it is also found that the maser line shifts towards lower frequencies with increasing t_{int}. This result also follows from the developed model: the red-shift increases with t_{int} since a longer interaction time leads to a more adiabatic behavior in the same way as a larger N_{ex} does.

The calculations reveal that on the vertical steps displayed in the signal the photon number distribution has two distinctly separate maxima similar to those observed at the phase transition points discussed above. Therefore, the maser field should exhibit hysteresis and metastability under the present conditions as well. The hysteresis indeed shows up when the cavity frequency is linearly scanned up and down with a modest scan rate [10]. When the maser is operated in steady-state and the cavity frequency is fixed to the steep side of one of the fringes we also observe spontaneous jumps of the maser field between two metastable field states.

The calculations also show that on the smooth wings of the more pronounced interference fringes the photon number distribution P(n) of the maser field is strongly sub-Poissonian. This leads us to the conclusion that we observe Ramsey-type interferences induced by a non-classical radiation field. The sub-Poissonian character of P(n) results from the fact that on the smooth wings of the fringes the photon gain reduces when the photon number is increased. This feedback mechanism stabilizes the photon number resulting in a sub-Poissonian photon distribution.

2.2 Entanglement in the Micromaser

Owing to the interaction of the Rydberg atom with the maser field there is an entanglement between field and state in which a particular atom is leaving the cavity.

This entanglement was studied in several papers, see e.g. Refs. [18] and [8]. Furthermore there is a correlation between the states of the atoms leaving the cavity subsequently. If e.g. atoms in the lower maser level are studied [19] an anticorrelation is observed in a region for the pump parameter Θ where sub-Poissonian photon statistics is present in the maser field. Recently measurements [20] of these pair correlations have been performed giving a rather good agreement with the theoretical predictions by Briegel et al. [21]. The pair correlations disappear when the time interval between subsequent atoms get larger than the storage time of a photon in the cavity.

2.3 The One-Atom Maser and Ultracold Atoms

In the following chapter we discuss the case that the micromaser is pumped by ultracold atoms; in this limit the center of mass motion has to be treated quantum mechanically, especially when the kinetic energy $(\hbar k)^2/2M$ of the atoms is of the same order or smaller than the atom-field [22] interaction energy $\hbar\Omega$.

For simplicity, we here consider the situation where an atom in the excited state $|e\rangle$ is incident upon a cavity that contains n photons so that the combined atom-field system is described by the state $|e,n\rangle =$

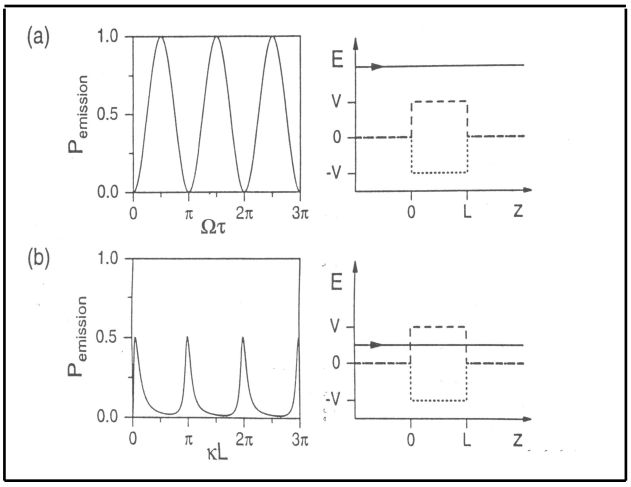

Figure 5: *Emission probability for (a) thermal atoms with k/κ=10 versus the interaction time Ωτ and (b) ultracold atoms with k/κ=0.1 versus the interaction length κL, and the corresponding repulsive (dashed) and attractive (dotted) atom-field potential. The constant κ is defined by* $(\hbar\kappa)^2/2m = \hbar\Omega$.

$(|\gamma_{n+1}^+\rangle + |\gamma_{n+1}^-\rangle)/\sqrt{2}$. The dressed-state components $|\gamma_{n+1}^+\rangle$ and $|\gamma_{n+1}^-\rangle$, which are the eigenstates of the atom-field interaction Hamiltonian, encounter different potentials giving rise to different reflection and transmission of the atom. Appropriate relative phase shifts between the dressed-state components during the atom-field interaction may result in the state $(|\gamma_{n+1}^+\rangle - |\gamma_{n+1}^-\rangle)/\sqrt{2} = |g, n+1\rangle$, which corresponds to the emission of a photon and a transition to the lower atomic level $|g\rangle$. Likewise, changes in the relative reflection and transmission amplitudes may lead to a de-excitation of the atom.

For thermal atoms, the emission probability shown in Fig. 5 displays the usual Rabi oscillations as a function of the interaction time τ. For very slow atoms, however, the emission probability is a function of the interaction length L and shows resonances such as the ones observed in intensity transmitted by a Fabry-Perot resonator. The resonances occur when the cavity length is an integer multiple of half the de Broglie wavelength of the atom inside the potential well.

Figure 6 illustrates the reflection and transmission of the atom for a cavity whose mode function is a mesa function, which approximates the lowest TM mode of a cylindrical cavity. For very cold atoms, the dressed-state component that encounters the potential barrier is always reflected. In general, the other dressed-state component is also reflected at the well. The situation changes dramatically if the cavity length is an integer multiple of half the de Broglie wavelength. In this case, the $|\gamma_{n+1}^-\rangle$ is completely

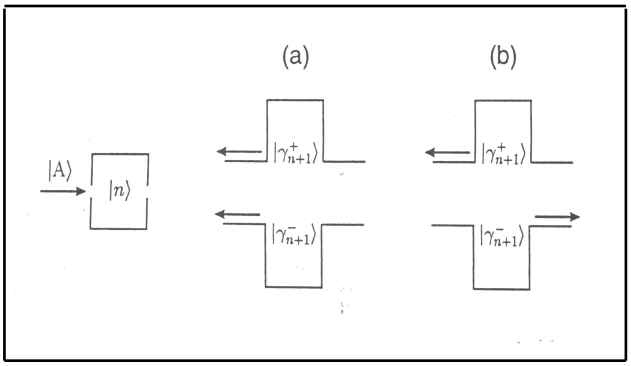

Figure 6: *Reflection and transmission of the atoms at the potential barrier for the* $|\gamma_{n+1}^{+}\rangle$ *and at the potential well for the* $|\gamma_{n+1}^{-}\rangle$ *component (a) out of the mazer resonance and (b) on resonance.*

transmitted, which implies a 50% transmission probability for the atom. A detailed calculation [22] shows that in such a situation the emission probability for a photon is 1/2 for each of the two dressed-state components, yielding an overall emission probability $P_{emission} = 1/2$.

So far, we have discussed the motion and atom-field interaction of a single atom incident upon the cavity. Due to the unusual emission probability, a beam of ultracold atoms can produce unusual photon distributions such as a shifted thermal distribution. For details about this microwave amplification by z-motion induced emission of radiation (mazer), the reader is referred to the trilogy [23-25].

In order to see the mazer resonances for atoms with a certain velocity spread, the interaction length L has to be small. Whereas in the usual cylindrical micromaser cavities the smallest cavity length is given by half the wavelength of the microwaves, cavities of the reentrant type, as depicted in Fig. 7, allow for an interaction length much smaller than the wavelength. With such a device, an experiment with realistic parameters seems possible [24].

3 Ion Trap Experiments

Besides the experiments performed with atoms in a cavity the trapped ion techniques provide another way to investigate quantum phenomena in radiation atom interaction. In the following recent experiments and new proposals for experiments will be reviewed.

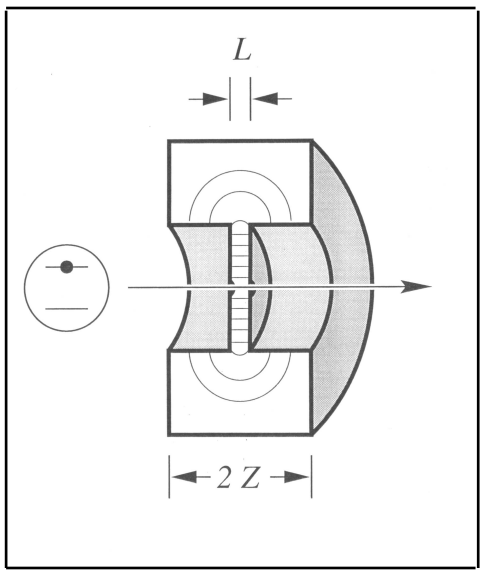

Figure 7: *Possible experimental setup with a reentrant cavity.*

3.1 Resonance Fluorescence of a Single Atom

Resonance fluorescence of an atom is a basic process in radiation-atom interactions, and has therefore always generated considerable interest. The methods of experimental investigation have changed continuously due to the availability of new experimental tools. A considerable step forward occurred when tunable and narrow band dye laser radiation became available. These laser sources are sufficiently intense to easily saturate an atomic transition. In addition, the lasers provide highly monochromatic light with coherence times much longer than typical natural lifetimes of excited atomic states. Excitation spectra with laser light using well collimated atomic beam lead to a width being practically the natural width of the resonance transition, therefore it became possible to investigate the frequency spectrum of the fluorescence radiation with high resolution. However, the spectrograph used to analyze the reemitted radiation was a Fabry-Perot interferometer, the resolution of which did reach the natural width of the atoms, but was insufficient it reach the laser linewidth, see e.g. Hartig et al. [26] and Cresser et al. [27]. A considerable progress in this direction was achieved by investigating the fluorescence spectrum of ultra-cold atoms in an optical lattice in a heterodyne experiment [28]. In these measurements a linewidth of 1 kHz was achieved, however, the quantum aspects of the resonance fluorescence such as antibunched photon statistics cannot be investigated under these conditions since they wash out when more than one atom is involved.

Thus the ideal experiment requires a single atom to be investigated. Since some time it is known that ion traps allow to study the fluorescence from a single laser cooled particle practically at rest, thus providing the ideal case for the spectroscopic investigation of the resonance fluorescence. The other essential ingredient for achievement of high resolution is the measurement of the frequency spectrum by heterodyning the scattered radiation with laser light as demonstrated with many cold atoms [28]. Such an optimal experiment with a single trapped Mg^+ ion is described in this paper. The measurement of the spectrum of the fluorescent radiation at low excitation intensities is presented. Furthermore, the photon correlation of the fluorescent light has been investigated under practically identical excitation conditions. The comparison of the two results shows a very interesting aspect of complementarity since the heterodyne measurement corresponds to a "wave" detection of the radiation whereas the measurement of the photon correlation is a "particle" detection scheme. It will be shown that under the same excitation conditions the wave detection provides the properties of a classical atom, i.e. a driven oscillator, whereas the particle or photon detection displays the quantum properties of the atom. Whether the atom displays classical or quantum properties thus depends on the method of observation.

The spectrum of the fluorescence radiation is given by the Fourier transform of the first order correlation function of the field operators, whereas the photon statistics and photon correlation is obtained from the second order correlation function. The corresponding operators do not commute, thus the respective observations are complementary. Present theory on the spectra of fluorescent radiation following monochromatic laser excitation can be summarized as follows: fluorescence radiation obtained with low incident intensity is also monochromatic owing to energy conservation. In this case, elastic scattering dominates the spectrum and thus one should measure a monochromatic line at the same frequency as the driving laser field. The atom stays in the ground state most of the time and absorption and emission must be considered as one process with the atom in principle behaving as a classical oscillator. This case was treated on the basis of a quantized field many years ago by Heitler [29]. With increasing intensity upper and lower states become more strongly coupled leading to an inelastic component, which increases with the square of the intensity. At low intensities, the elastic part dominates since it depends linearly on the intensity. As the intensity of the exciting light increases, the atom spends more time in the upper state and the effect of the vacuum fluctuations comes into play through spontaneous emission. The inelastic component is added to the spectrum, and the elastic component goes through a maximum where the Rabi flopping frequency $\Omega = \Gamma / \sqrt{2}$ (Γ is the natural linewidth) and then disappears with growing Ω. The inelastic part of the spectrum gradually broadens as Ω increases and for $\Omega > \Gamma/2$ sidebands begin to appear [27,

30].

The experimental study of the problem requires, as mentioned above, a Doppler-free observation. In order to measure the frequency distribution, the fluorescent light has to be investigated by means of a high resolution spectrometer. The first experiments of this type were performed by Schuda et al. [31] and later by Walther et al. [32], Hartig et al. [26] and Ezekiel et al. [33]. In all these experiments, the excitation was performed by single-mode dye laser radiation, with the scattered radiation from a well collimated atomic beam observed and analyzed by a Fabry-Perot interferometer.

Experiments to investigate the elastic part of the resonance fluorescence giving a resolution better than the natural linewidth have been performed by Gibbs at al. [34] and Cresser at al. [27].

The first experiments which investigated antibunching in resonance fluorescence were also performed by means of laser-excited collimated atomic beams. The initial results obtained by Kimble, Dagenais, and Mandel [35] showed that the second-order correlation function $g^{(2)}$ (t) had a positive slope which is characteristic of photon antibunching. However, $g^{(2)}$ (0) was larger than $g^{(2)}$ (t) for $t \to \infty$ due to number fluctuations in the atomic beam and to the finite interaction time of the atoms [36, 37]. Further refinement of the analysis of the experiment was provided by Dagenais and Mandel [37]. Rateike et al. [38] used a longer interaction time for an experiment in which they measured the photon correlation at very low laser intensities (see Cresser at al. [27] for a review). Later, photon antibunching was measured using a single trapped ion in an experiment which avoids the disadvantages of atom number statistics and finite interaction time between atom and laser field [39].

As pointed out in many papers antibunching is a purely quantum phenomenon (see e. g. Cresser et al. [27] and Walls [40]). The fluorescence of a single ion displays the additional nonclassical property that the variance of the photon number is smaller than its mean value (i.e. it is sub-Poissonian) [39, 41].

The trap used for the present experiment was a modified Paul-trap, called an endcap-trap [42]. The trap consists of two solid copper-beryllium cylinders (diameter 0.5 mm) arranged co-linearly with a separation of 0.56 mm. These correspond to the cap electrodes of a traditional Paul trap, whereas the ring electrode is replaced by two hollow cylinders, one of which is concentric with each of the cylindrical endcaps. Their inner and outer diameters are 1 and 2 mm, respectively and they are electrically isolated from the cap electrodes. The fractional anharmonicity of this trap configuration, determined by the deviation of the real potential from the ideal quadrupole field is below 0.1% (see Schrama et al. [42]). The trap is driven at a frequency of 24 MHz with typical secular frequencies in the xy-plane of approximately 4 MHz. This required a radio-frequency voltage with an

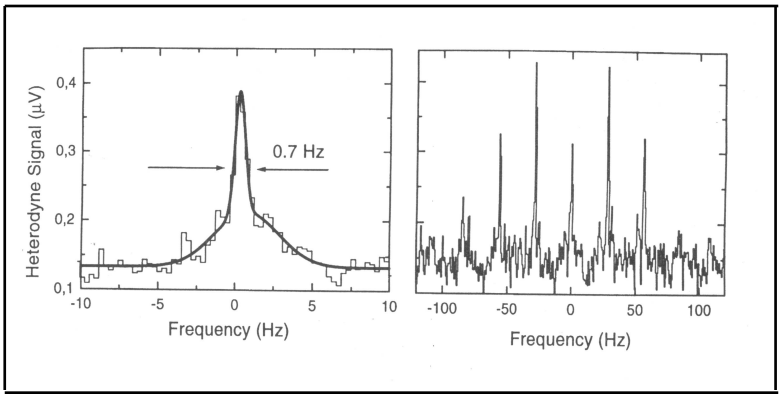

Figure 8: *Heterodyne spectrum of a single trapped 24 Mg^+-ion. Left side: Resolution bandwidth 0.5 Hz. The solid line is a Lorentzian fit to the experimental data; the peak appears on top of a small pedestal being 4 Hz wide. The latter signal is due to random phase fluctuations in the spatially separated sections of the light paths of local oscillator and fluorescent light; they are generated by variable air currents in the laboratory. Right side: Heterodyne spectrum of the coherent peak with sidebands generated by mechanical vibrations of the mount holding the trap. The vibrations are due to the operation of a rotary pump in the laboratory. For details see Ref. [44].*

amplitude on the order of 300 V to be applied between the cylinders and the endcaps.

The measurements were performed using the $3^2S_{1/2}$ - $3^2P_{3/2}$ transition of $24Mg^+$ - ion at a wavelength of 280 mm. The heterodyne measurement is performed as follows. The dye laser excites the trapped ion while the fluorescence is observed in a direction of about 54° to the exciting laser beam. However, both the observation direction and the laser beam are in a plane perpendicular to the symmetry axis of the trap. A fraction of the laser radiation is removed with a beamsplitter and then frequency shifted (by 137 MHz with an acousto-optic modulator (AOM)) to serve as the local oscillator. An example of a heterodyne signal is displayed in Fig. 8. The signal is the narrowest optical heterodyne spectrum of resonance fluorescence reported to date. Thus our experiment provides the most compelling confirmation of Weisskopf's prediction of a coherent component in resonance fluorescence. The linewidth observed implies that exciting laser and fluorescent light are coherent over a length of 400 000 km. Further details on the experiment are given in Refs. [43] and [44].

Investigation of photon correlations employed the ordinary Hanbury-Brown and Twiss setup. The setup was essentially the same as described by Diedrich and Walther [39]. The results are shown and discussed in Ref. [43] also.

The presented experiment describes the first high-resolution heterodyne measurement of the elastic peak in resonance fluorescence of a single ion. At identical experimental parameters we also measured antibunching in the photon correlation of the scattered field. Togheter, both measurements show that, in the limit of weak excitation, the fluorescence light differs from the excitation radiation in the second-order correlation but not in the first order correlation. However, the elastic component of resonance fluorescence combines an extremely narrow frequency spectrum with antibunched photon statistics, which means that the fluorescence radiation is not second-order coherent as expected from a classical point of view [45]. The heterodyne and the photon correlation measurement are complementary since they emphasize either the classical wave properties or the quantum properties of resonance fluorescence, respectively.

3.2 The Ion-Trap Laser

There have been several theoretical papers on one-atom lasers in the past [46-49, 56]. This system provides a testing ground for new theoretical concepts and results in the quantum theory of the laser. Examples are atomic coherence effects [50] and dynamic (i.e. self-generated) quantum-noise reduction [51, 52, 49]. All these aspects are a consequence of a pump process whose complex nature is not accounted for in the standard treatment of the laser. So far there is one experiment where laser action could be demonstrated with one atom at a time in the optical resonator [6]. A weak beam of excited atoms was used to pump this one-atom laser.

A formidable challenge for an experiment is to perform a similar experiment with a trapped ion in the cavity. Mirrors with an ultrahigh finesse are required, and a strong atom-field coupling is needed. After the emission of a photon, the ion has to be pumped before the next stimulated emission can occur. Similar as in the resonance fluorescence experiments which show antibunching, [35, 39] there is a certain time gap during which the ion is unable to add another photon to the laser field. It has been shown [49] that this time gap plays a significant role in the production of a field with sub-Poissonian photon statistics.

We have investigated the theoretical basis for an experimental realization of the ion-trap laser. Our analysis takes into account details such as the multi-level structure, the coupling strenghts and the parameters of the resonator. It has been a problem to find an ion with an appropriate level scheme. We could show that it is possible to produce a laser field with the parameters of a single Ca^+ ion. This one-atom laser displays several features, which are not found in conventional lasers: the development of two thresholds, sub-Poissonian statistics, lasing without inversion and self-quenching. The details of this work are reported in Ref. [53, 54]. In a subsequent paper [55] also the center-of-mass motion of the trapped ion was

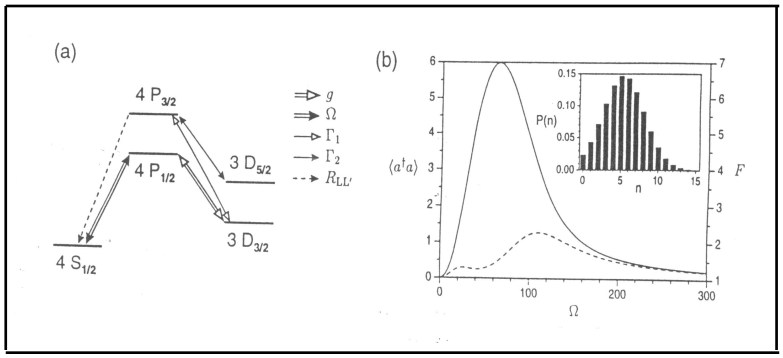

Figure 9: *(a) Schematic representation of the Ca^+ scheme for the ion-trap laser. (b) Means photon number $\langle a^\dagger a\rangle$ (solid) and Fano factor F (dashed) versus the coherent pump strength* Ω. *The parameters are* $A = 1$, $g = 14.8$, $\Gamma_1 = 40$, *and* $\Gamma_2 = 100$. *The inset shows the photon distribution for* $\Omega = 50$. *All rates are in MHz.*

quantized. This leads to additional features of the ion trap laser, especially a multiple vacuum Rabi-splitting is observed.

The Ca^+ scheme is sketched in Fig. 9(a). It contains a Λ-type subsystem: the ion is pumped coherently from the ground state to the upper laser level $4P_{1/2}$, stimulated emission into the resonator mode takes place on the transition to $3D_{3/2}$ at a wavelength of 866 mm. Further pump fields are needed to close the pump cycle and to depopulate the metastable levels.

Although spontaneous relaxation from the upper laser level to the ground state takes place at a relatively large rate of 140 MHz and suppresses the atomic polarization on the laser transition, laser light is generated for realistic experimental parameters due to atomic coherence effects within the Λ subsystem. The occurrence of laser action is demonstrated in Fig. 9(b) for a resonator with a photon damping rate A=1 MHz and a vacuum Rabi frequency g=14.8 MHz on the laser transition. For the numerical calculation of the realistic scheme, the Zeeman substructure and the polarizations of the fields have to be taken into account. With increasing coherent pump Ω, the mean photon number inside the resonator first increases and then decreases. Both the increase and decease of the intensity are accompanied by maxima in the intensity fluctuations, which can be interpreted as thresholds. Laser action takes place in between these two thresholds. This is confirmed by the Poissonian-like photon distribution given in the inset of Fig. 9(b). In addition, the linewidth of the output spectrum is in the laser region up to ten times smaller than below the first and beyond the second threshold [54]. Note that for a thermal distribution the solid and dashed curves in Fig. 9(b) for the intensity and the intensity fluctuations would coincide.

For a nonvanishing Lamb-Dicke parameter η, higher vibrational states

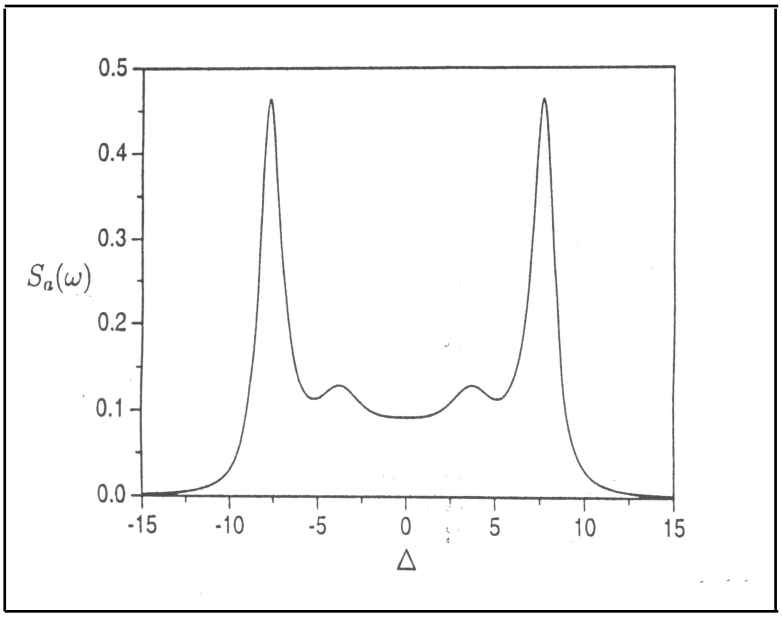

Figure 10: *Multiple vacuum Rabi splitting in the output spectrum* $S_a(\omega)$ *for the two level atom with quantized CM motion. The parameters are* $A = 0.1$, $B = 0.05$, $\mu = 0.5$, $R_{AB} = 0.1$, $R_{BA} = 0.001$, *and* $\eta = 0.7$. *All rates are in units of* g_0.

will be excited during the pump and relaxation processes; the amplitude of the atomic motion will increase. Therefore, the ion will in general not remain at an antinode of the resonator mode, and the strength of the atom-field coupling will decrease. However, the atom can be prevented from heating up by detuning a coherent pump field. The coupling strength is given by the product of a constant g_0 and a motion-dependent function [55] that is determined by an overlap integral involving the motional wave function of the atom and the mode function of the field.

In a simple two-level laser model with decay rate R_{AB} and pump rate R_{BA}, the cooling process may be incorporated by coupling the atomic motion to a thermal reservoir with cooling rate B and thermal vibron number μ. Already in such a simple model, the discrete nature of the quantized motion shows up below threshold in a multiple vacuum Rabi splitting of the output spectrum [55]. This is illustrated in Fig. 10. The pairs of peaks correspond to different vibrational states with different atom-field coupling.

The cooling mechanism is most transparent in the special case of resolved sideband cooling. The coherent pump may be detuned to the first lower vibrational sideband so that with each excitation from $4S_{1/2}$ to $4P_{1/2}$ one vibron is annihilated and the CM motion is cooled. Eventually, all the

population will collect in the motional ground state of the atomic ground state $4S_{1/2}$ and cannot participate in the lasing process. The coherent pump strength is now given by Ω_0 times a motion-dependent function. In order to maintain laser action in the presence of the cooling, an additional broadband pump field Γ may be applied to the cooling transition. Figure 11 indicates that a field with a mean photon number $\langle a^\dagger a \rangle = 2.3$ is generated while the mean vibron number is restricted to a value of $\langle b^\dagger b \rangle = 0.5$. If a larger mean vibron number is acceptable, the pump rate Γ can be increased and more population takes part in the laser action. This leads to considerably larger mean photon numbers. The calculation shows that it is possible to incorporate a cooling mechanism in a multilevel one-atom laser scheme and to obtain significant lasing also for nonperfect localization of the atom. Although it is difficult to reach the resolved-sideband limit in an experiment, cooling may still be achieved in the weak-binding regime by detuning a coherent pump field.

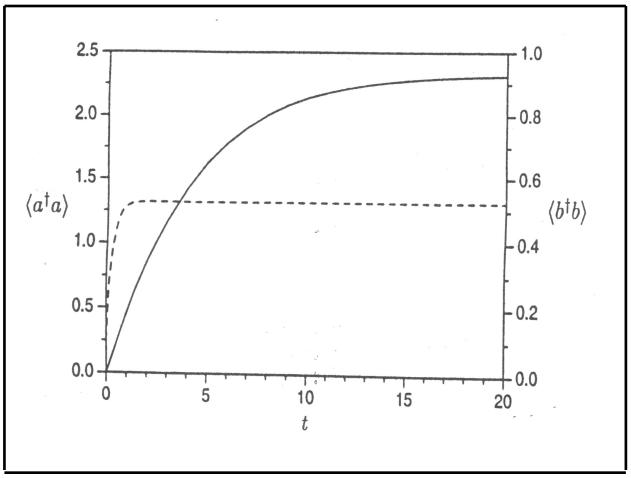

Figure 11: *Time evolution of the mean photon number (solid) and the mean vibron number (dashed) in the Ca^+ ion-trap laser with sideband cooling. The parameters are $A = 0.5$, $g_0 = 14.8$, $\Omega_0 = 100$, $\Gamma = \Gamma_1 = 40$, $\Gamma_2 = 100$, and $\eta = 0.1$ on the laser transition. Initially, the atom is in the ground state and the vibronic distribution is thermal with $\langle b^\dagger b \rangle = 0.1$. All rates are in MHz.*

4 Conclusions

In this paper recent experiments with single atoms in cavities and traps are reviewed. It is especially pointed out that using ultracold atoms will lead to new interesting aspects in atom-matter interaction. The possibility that

now ultracold atoms are available bring such experiments into reach in the near future.

The quantum-mechanical CM motion of the atoms incident upon a micromaser cavity is equivalent to a scattering problem that involves both a repulsive and an attractive potential. The emission probability for an initially excited ultracold atom exhibits sharp resonances when the de Broglie wavelength fits resonantly into the cavity. These resonances may be observed experimentally with the help of a reentrant cavity. Whereas the eigenstates of the atomic motion are continuously distributed for the maser, the motion is confined to a trapping potential in the one-atom laser. The discrete nature of the CM motion in the trap is reflected below threshold by multiple vacuum Rabi splitting. In order to prevent the atom from being continuously heated by the pump and relaxation processes, sideband cooling has been incorporated into the model. The recently proposed Ca^+ ion-trap laser is used to illustrate the possibility of one-atom lasing in the presence of a cooling mechanism.

There is one very interesting application of the "mazer" which should be briefly mentioned here: the device can act as a filter for matter waves and can thus be used to increase the coherence length of an atomic beam; in the same way as a Fabry-Perot can be used to increase the coherence length of a light wave. This application will be discussed in a forthcoming paper [57].

References

[1] MESCHEDE D., WALTHER H. and MÜLLER G., Phys. Rev. Lett. 54, 551 (1985)

[2] REMPE G., WALTHER H. and KLEIN N., Phys Rev. Lett. 58, 353 (1987)

[3] REMPE G., SCHMIDT-KALER F. and WALTHER H., Phys. Rev. Lett. 64, 2783 (1990)

[4] REMPE G. and WALTHER H., Phys. Rev. A 42, 1650 (1990)

[5] KIMBLE H.J., CARNAL O., GEORGIADES N., MABUCHI H., POLZIK E.S., THOMPSON R.J. and TURCHETTE Q.A., *"Atomic Physics"*, (edited by D.J. Wineland, C.E. Wieman, S.J. Smith) (American Institute of Physics, New York 1995), vol. **14**, p. 314

[6] AN K., CHILDS J.J., DASARI R.R., FELD M.S., Phys. Rev. Lett. **73**, 3375 (1994)

[7] WAGNER C., BRECHA R.J., SCHENZLE A., and WALTHER H., Phys. Rev. A **47**, 5068 (1993)

[8] LÖFFLER M., ENGLERT B.G. and WALTHER H., Appl. Phys. B 63, 511 (1996)

[9] BENSON O., RAITHEL G., and WALTHER H., Phys. Rev. Lett. **72**, 3506 (1994)

[10] RAITHEL G., BENSON O. and WALTHER H., Phys. Rev. Lett. **75**, 3446 (1995)

[11] RAITHEL G., WAGNER C., WALTHER H., NARDUCCI L.M. and SCULLY M.O., *"Advances in Atomic, Molecular, and Optical Physics"* , Supplement 2, (Edited by P. Berman) (Academic Press, New York 1994), p. 57

[12] FILIPOWICZ P., JAVANAINEN J. and MEYSTRE P., Phys. Rev. A **34**, 3077 (1986)

[13] LUGIATO L.A., SCULLY M.O. and WALTHER H., Phys. Rev. A **36**, 740 (1987)

[14] MEYSTRE P., *"Progress in Optics"*, (Edited by E. Wolf) (Elsevier Science Publishers, New York 1992), Vol. **30**, p. 261

[15] RAIMOND J.M., BRUNE M., DAVIDOVICH L., GOY P. and HAROCHE S., Atomic Physics 11, 441 (1989)

[16] RAMSEY N.F., *"Molecular Beams"*, (Clarendon Press, Oxford 1956), p. 124

[17] COHEN-TANNOUDJI C., DUPONT-ROC J. and GRYNBERG G., *"Atom-Photon Interactions"*, (John Wiley and Sons, Inc., New York 1992), p. 407

[18] WAGNER C., SCHENZLE A. and WALTHER H., Optics Communications 107, 318 (1994)

[19] WALTHER H., Phys. Reports **219**, 263 (1992)

[20] WEIDINGER M., BENSON O. and WALTHER H., to be published

[21] BRIEGEL H.-J., ENGLERT B.-G., STERPI N. and WALTHER H., Phys. Rev. A 49, 2962 (1994)

[22] SCULLY M.O., MEYER G.M., and WALTHER H., Phys. Rev. Lett. **76**, 4144 (1996)

[23] MEYER G.M., SCULLY M.O. and WALTHER H., Phys. Rev. A, in print

[24] LÖFFLER M., MEYER G.M., SCHRÖDER M., SCULLY M.O. and WALTHER H., Phys. Rev. A, in print

[25] SCHRÖDER M., VOGEL K., SCHLEICH W.P., SCULLY M.O. and WALTHER H., Phys. Rev. A, in print

[26] HARTIG W., RASMUSSEN W., SCHIEDER R. and WALTHER H., Z. Physik A278, 205 (1976)

[27] CRESSER J.D., HÄGER J., LEUCHS G., RATEIKE F.M. and WALTHER, H., Topics in Current Physics 27, 21 (1982)

[28] JESSEN P.S., GERZ C., LETT P.D., PHILIPPS W.D., ROLSTON S.L., SPREUUW R.J.C. and WESTBROOK C.I., Phys. Rev. Lett. 69, 49 (1992)

[29] HEITLER W., *"The Quantum Theory of Radiation"*, Third Edition, (University Press, Oxford 1954), p. 196

[30] MOLLOW B.R., Phys. Rev. 188, 1969 (1969)

[31] SCHUDA F., STROUD C. JR. and HERCHER M., J. Phys. B1, L198 (1974)

[32] WALTHER H., Lecture Notes in Physics 43, 358 (1975)

[33] WU F.Y., GROVE R.E. and EZEKIEL S., Phys. Rev. Lett. 35, 1426 (1975); GROVE R.E., WU F.Y. and EZEKIEL S., Phys. Rev. Lett. A 15, 227 (1977)

[34] GIBBS H.M. and VENKATESAN T.N.C., Opt. Comm. 17, 87 (1976)

[35] KIMBLE H.J., DAGENAIS M. and MANDEL L., Phys. Rev. Lett. 39, 691 (1977)

[36] JAKEMAN E., PIKE E.R., PUSEY, P.N. and VAUGHAM J.M., J. Phys. A 10, L257 (1977)

[37] KIMBLE H.J., DAGENAIS M. and MANDEL L., Phys. Rev. A 18, 201 (1978); DAGENAIS M. and MANDEL L., Phys. Rev. A 18, 2217 (1978).

[38] RATEIKE F.M., LEUCHS G. and WALTHER H., results cited in Ref. 21

[39] DIEDRICH F. and WALTHER H., Phys. Rev. Lett. 58, 203 (1987)

[40] WALLS D.F., Nature 280, 451 (1979)

[41] SHORT R. and MANDEL L., Phys. Rev. Lett. **51, 384** (1983), and in *"Coherence and Quantum Optics"*, (Edited by L. Mandel and E. Wolf) (Plenum, New York 1984), vol. V, p. 671

[42] SCHRAMA C.A., PEIK E., SMITH WW. and WALTHER H., Opt. Comm. 101, 32 (1993)

[43] HÖFFGES J.T., BALDAUF H.W., EICHLER T., HELMFRID S.R. and WALTHER, H., Opt. Communications 133, 170 (1997)

[44] HÖFFGES J.T., BALDAUF H.W., LANGE W. and WALTHER H., Journal of Modern Optics, in print

[45] LOUDON R., Rep. Progr. Phys. 43, 913 (1980)

[46] MU Y. and SAVAGE C.M., Phys. Rev. A 46, 5944 (1992)

[47] GINZEL C., BRIEGEL H.-J., MARTINI U., ENGLERT B-G. and SHENZLE, A., Phys. Rev. A 48, 732 (1993)

[48] PELLIZZARI T. and RITSCH H., J. Mod. Opt. 41, 609 (1994); Phys. Rev. Lett. 72, 3973 (1994); Horak P., Gheri K.M. and Ritsch H., Phys. Rev. A 51, 3257 (1995)

[49] BRIEGEL H.-J., MEYER G.M. and ENGLERT B.-G., Phys. Rev. A 53, 1143 (1996); Europhys. Lett. 33, 515 (1996)

[50] For a recent review see ARIMONDO E., "Progress in Optics", (Edited by E. Wolf) (Elsevier, Amsterdam 1996), vol. XXXV, p. 257

[51] KHAZANOV A.M., KOGANOV G.A. and GORDOV E.P., Phys. Rev. A 42, 3065 (1990); Ralph T.C. and Savage C.M., Phys. Rev. A 44, 7809 (1991); Ritsch H., Zoller P., Gardiner C.W. and Walls D.F., Phys. Rev. A 44, 3361 (1991)

[52] GHERI K.M. and WALLS D.F., Phys. Rev. A 45, 6675 (1992); Ritsch H. and Marte, M.A.M., Phys. Rev. A 47, 2354 (1993)

[53] MEYER G.M., BRIEGEL H.-J. and WALTHER H., Europhys. Lett. 37, 317 (1997)

[54] MEYER G.M., LÖFFLER M. and WALTHER H., Phys. Rev. A 56, R 1099 (1997)

[55] LÖFFLER M., MEYER G.M. and WALTHER H., to be published

[56] LÖFFLER M., MEYER G.M. and WALTHER H., Phys. Rev. A 55, 3923 (1997)

[57] LÖFFLER M. and WALTHER H., to be published

Herbert Walther
Sektion Physik der Universität München
Max-Planck-Institut für Quantenoptik
85748 Garching, Fed. Rep. of Germany
e-mail: Herbert.Walther@mpq.mpg.de